PERGAMON

Acta mater. Vol. 47, No. 10, pp. 2913–2926, 1999

PII: S1359-6454(99)00153-6
1359-6454/99 $20.00 + 0.00

NONLINEAR ELECTRIC–MECHANICAL BEHAVIOR AND MICROMECHANICS MODELLING OF FERROELECTRIC DOMAIN EVOLUTION

W. LU, D.-N. FANG†, C. Q. LI and K.-C. HWANG

Failure Mechanics Laboratory, Department of Engineering Mechanics, Tsinghua University, Beijing 100084, People's Republic of China

(Received 14 August 1998; accepted 13 May 1999)

Abstract—Domains exist in ferroelectric ceramics. External loads, such as electric field and stress, can cause domain switching. Domain switching always results in nonlinear ferroelectricity and ferroelasticity of ferroelectric ceramics. In this investigation, nonlinear electric–mechanical behavior related to ferroelectric and ferroelastic domain switching is experimentally and theoretically studied. In the experimental work, the electric–mechanical response of a soft PZT ferroelectric ceramic subjected to combined electric–mechanical loads was observed. The effect of different compressive stress levels on the electromechanical response was examined. In the theoretical modelling, the orientation of each domain is defined by its local coordinate relative to a fixed global coordinate. Orientation distribution function (ODF) is used to describe the domain pattern. For mathematical simplicity, the Reuss average is used in the modelling. According to the proposed theory, a domain has different Gibbs' energy at different orientation states and the energy difference forms the domain switching driving force. The domain pattern and its evolution are determined by the joint action of the domain switching driving force and the dissipation during domain switching. In ferroelectricity and ferroelasticity, 90° and 180° domain switchings play different roles and have different switching dissipations associated with them. A criterion considering the difference between the 90° switching and the 180° switching is established by the thermodynamic approach. There is an agreement between theoretical and experimental results. It should be pointed out that the micromechanical model proposed in this paper is restricted to ferroelectric materials exhibiting transformation from cubic to tetragonal only. © *1999 Acta Metallurgica Inc. Published by Elsevier Science Ltd. All rights reserved.*

Keywords: Constitutive equations; Ferroelectricity; Functional ceramics; Piezoelectricity

1. INTRODUCTION

Ferroelectric ceramics have found many applications after years of development [1–4]. The perovskite type ceramics are a very important class of them. Examples are $BaTiO_3$, PZT and PLZT, etc. [1]. A common feature of them is that they all have ABO_3 structures. Figure 1 gives a simple illustration. A unit cell of this structure has an A^{2+} ion at each corner, a B^{4+} ion at the body center and an O^{2-} ion at each face center. The shape and properties of such a unit cell is affected by temperature. When the temperature is above the Curie point, the unit cell is cubic and the ions lie symmetrically in it. Both the positive and the negative charge centers coincide with the cube center, as shown in Fig. 1(a), and the unit cell does not show polarization. This higher symmetry prototype phase is paraelectric. Phase transition will occur when the temperature goes down to the Curie point. During the course of phase transition, the central B^{4+} ion moves relative to the surrounding O^{2-} ions and results in a shape change of the unit cell. The symmetry decreases and the unit cell changes to tetragonal, as shown in Fig. 1(b). The shape change of the unit cell leads to a spontaneous strain relative to the paraelectric cubic phase. Another effect of the relative displacement of ions is that the positive and the negative charge centers no longer coincide with each other and a spontaneous polarization appears. The unit cells in a ferroelectric ceramic that have the same spontaneous polarization form a ferroelectric domain. Domain switching is the main source of nonlinearity in ferroelectric ceramics.

An electric field can switch a domain by either 180° or 90°, while a stress can switch a domain by only 90°. A 180° domain switching can cause a direct change of polarization and at the same time leads to a change of piezoelectric compliance tensor. This change of the piezoelectric compliance tensor can induce a change of strain. When the polarization is in the same direction as the electric field, the unit cell elongates along its *c* edge. When polarization is in the direction opposite to the electric field, the unit cell contracts its *c* edge. A 90° domain switching can cause a direct change of both polarization and strain. If the domain is not dielectric isotropic, the 90° domain switching will also lead to an additional change of polarization related to the change of dielectric tensor. The coupling of

†To whom all correspondence should be addressed.

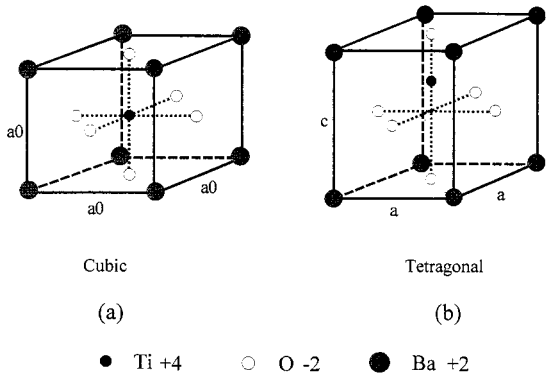

Fig. 1. Crystal structure of $BaTiO_3$.

the mechanical and electric effect will induce an additional linear change of polarization and strain. The 90° domain switching that occurs under stress can be analyzed in analogy to the 90° domain switching that occurs under electric field. Domain switching is associated with domain wall movements. Experiments show that when an electric or a mechanical load exceeds a certain value, the domain wall begins to move and the speed of its movement is related to the intensity of the load. Domain wall movements can lead to 90° or 180° domain switching [5–8]. The threshold for 90° or 180° domain switching is different, we will consider the difference in this paper.

As the applied field becomes larger, the strain deviates from linearity, and significant hysteresis appears because of the domain switching. The hysteresis limits the application of the ferroelectric ceramics, especially under a large applied electric or stress field. The study on the hysteresis can exhume the potential application of the materials [9, 10]. Ferroelectirc ceramics are susceptible to brittle fracture that can lead to catastrophic failure. Therefore, it is important to understand the deformation and fracture behavior of ferroelectric materials under coupled electromechanical fields [11]. One way to accomplish this is to resort to well-established linear elastic fracture mechanics [12–16]. On the other hand, a better understanding of the fracture behavior in PZT ceramics was obtained on the basis of the domain switching mechanisms and related theory of nonlinear fracture mechanics [11, 17]. Since the crack tip stress fields are singular, a nonlinear effect such as domain switching exists near the crack tip even though the remote field is less than the coercive value. This implies that the structure reliability concerns of electromechanical devices call for a better understanding of nonlinear constitutive laws of ferroelectric ceramics as well as related domain switching criteria. Some progress in modelling constitutive relations for ferroelectric materials has been made by many researchers, such as McMeeking [12], Suo [18], Yang and Suo [19], Hwang *et al.* [20], Lynch and McMeeking [21], Huo and Jiang [22], Loge and Suo [23], Chen *et al.* [24, 25], Lu *et al.* [26–28], and Michelitsch and Kreher [29], but no general constitutive laws are available for ferroelectrics [30]. The difficulties arise from hysteresis, multiaxial loading and anisotropic electric–mechanical coupling. The strain and electric displacement depend not only on the current stress and electric field, but also on the loading history.

Table 1. Main properties of the soft PZT-51 ceramic [32]

Material properties	Value
Elastic modulus (Pa)	3.03E10
Poisson's ratio	0.3
Dielectric permittivity, k_{33} (F/m)	6.666E−8
Piezoelectric coefficient, d_{333} (m/V)	1.52E−9
Piezoelectric coefficient, d_{311} (m/V)	−0.57E−9
Piezoelectric coefficient, d_{113} (m/V)	1.856E−9
Coercive electric field, E_c (MV/m)	0.676
Coercive stress, σ_c (MPa)	21.8
Remanent macroscopic strain, $\bar{\varepsilon}^R_{11}$, $\bar{\varepsilon}^R_{22}$	−1.4E−3
Remanent macroscopic strain, $\bar{\varepsilon}^R_{33}$	2.7E−3
Remanent polarization, P^R (C/m^2)	0.1938

In this paper a domain switching model is proposed. The macroscopic behavior of ferroelectric ceramics is obtained by averaging contributions of all domains. The domain orientation distribution function depicts domain patterns. We suppose that domains are independent of each other and the internal electric field and stress of each domain are equal to the external load. This Reuss type approximation [31] has been used by Hwang *et al.* [20] in their one-dimensional computational ferroelectric crystal simulation. Numerical results based on the theory proposed in this paper show that the assumption does not cause too much error and is acceptable. A more thorough investigation concerning the interaction of different domains needs the application of inclusion theory, a detailed discussion of this problem can be found in Refs [27, 28]. In order to verify the theory, the electric–mechanical response of a soft PZT ferroelectric ceramic subjected to combined electric–mechanical loads was experimentally observed. The effect of different compressive stress levels on the electromechanical response was examined as well. A criterion considering the difference between the 90° switching and the 180° switching is established by the thermodynamic approach. There is an agreement between the theoretical and the experimental results.

2. EXPERIMENTAL PROCEDURE

The material tested is a typical soft PZT-51 with large piezoelectric coefficients and dielectric permittivity [32]. Each grain of the ceramic is a single crystal with a tetragonal perovskite structure at room temperature. The published physical properties, the measured physical properties as well as the lattice constants of the soft PZT-51 ceramic are listed in Tables 1 and 2, respectively [32]. The specimens, with nominal dimensions $10 \times 10 \times 16\ mm^3$,

Table 2. Material lattice constants of the soft PZT-51 ceramic [28, 32]

Lattice constants, a_0, a, b, c of PZT-51 ceramic
$a_0 = 0.4071$ nm, $a = b = 0.4055$ nm, $c = 0.4102$ nm

were cut from bulk ferroelectrics, and all faces were polished. The upper and bottom faces of the specimens with an area of $10 \times 10\ \text{mm}^2$ were electroded with sputtered Ag. A servo-hydraulic loading fixture is set up for applying the stress field. A silicon oil bath is mounted on the loading fixture to prevent high voltage arcing. As a simple mechanical load, the stress field is applied to a polarized sample in the x_3-direction as shown in Fig. 2. Under combined electric–mechanical loads, unpolarized samples are subjected to a cyclic electric field parallel to the x_3-direction under different constant compressive stresses. As shown in Fig. 2, the sample is isolated from the fixture by two alumina blocks and one ethoxyline block. The high voltage arcing is prevented effectively by the silicon oil bath and a ringed ethoxyline block in the middle of the sample. To protect the strain gauges from the high voltage arcing, they must be bonded to the area near the ground electrode and covered by a special isolated glue. To avoid bending stress and inhomogeneous distribution of stress, the upper and bottom faces of both the alumina blocks and the ethoxyline block are kept parallel (misalignment less than 0.01 mm). Besides, one spherical cone is incorporated in the setup.

The load sensor output is recorded through an A/D circuit connected to the computer. Longitudinal and transverse strain gauges are bonded to the center of the area near the ground electrode to measure strains parallel and perpendicular to the polarization direction, i.e. x_3-direction. The strain gauges are connected to a Wheatstone bridge and the A/D circuit connected to the computer. The charge per unit area on the electrode is equal to the normal component of the electric displacement. The charge on the electrode is measured by monitoring the voltage of a capacitor

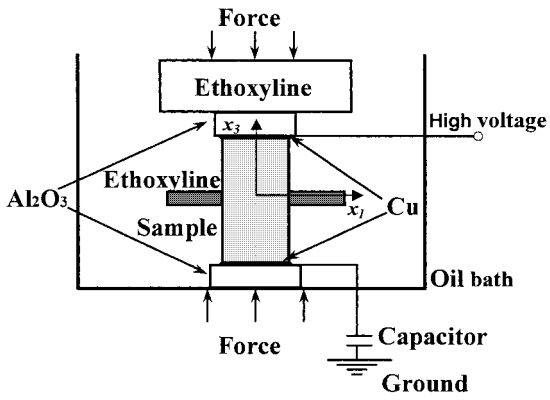

Fig. 2. Schematic of the electric–mechanical loading system.

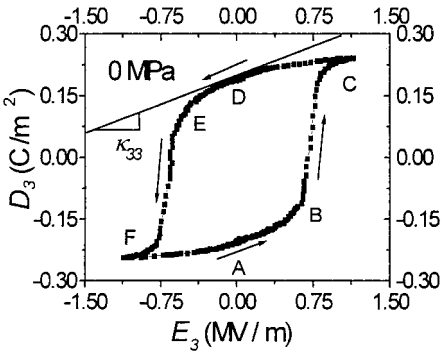

Fig. 3. Stable electric field vs electric displacement hysteresis loop.

(10 μF) connected from the bottom electrode of the specimen to the ground. The voltage of the capacitor is monitored by means of a high input impedance electrometer and the A/D circuit. A high voltage source triangle wave ($\pm$30 kV at from 1 to 0.01 Hz) is connected to the upper electrode of the specimen.

3. EXPRIMENTAL RESULTS

Initially unpolarized samples are subjected to a cyclic electric field parallel to the x_3-direction. Figure 3 shows the stable electric displacement–electric field curves measured after several load–unload cycles. In Fig. 3, D_3 and E_3 refer to the electric displacement and electric field in the direction of the x_3-axis, respectively. At point A the electric field is zero and the sample has a remanent polarization of $-0.194\ \text{C/m}^2$. A positive electric field (opposite to the direction of polarization) is applied to the sample. At point B, the electric field reaches the coercive field of 0.67 MV/m and the direction of polarization of the sample begins to switch. At point C, the polarization is almost aligned with the positive electric field. The electric field is reduced to zero at point D and the remanent polarization is $0.194\ \text{C/m}^2$. Then a negative electric field (opposite to the present direction of polarization) is applied to the sample and the electric displacement is reduced. At point E the electric field reaches the coercive field of -0.67 MV/m and the polarization starts to switch again. At point F the polarization is aligned with the present electric field. Finally, the electric field is reduced to zero and the state of the sample returns to that of point A. As the sample is in the polarized states of points A and D, the increment of electric displacement is linearly proportional to the small change of the electric field, which can be described by $\Delta D_3 = k_{33}\Delta E_3$. That is, the slope provides a relative permittivity of $k_r = k_{33}/k_0 = 7532$, where the permittivity of the free space is $k_0 = 8.85 \times 10^{-12}\ \text{F/m}$.

When the stable electric field vs electric displacement hysteresis is developed, the longitudinal strain, ε_{33}, and the transverse strain, ε_{11}, of the sample could be simultaneously measured. It should be

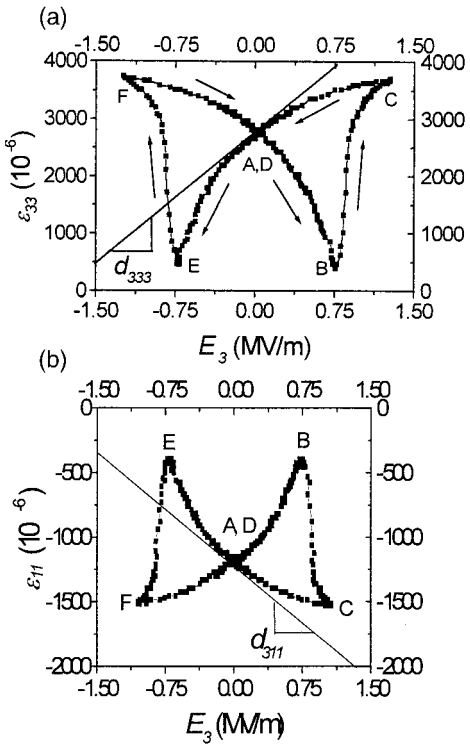

Fig. 4. Stable strain vs electric field curve (after several cycles): (a) longitudinal strain vs electric field; (b) transverse strain vs electric field.

pointed out that the ceramic is transversely isotropic. The polarization direction is parallel to the x_3-axis. Thus, the x_3-direction is specified as the longitudinal direction and the x_1–x_2 plane is a transverse plane. The stable electric field vs longitudinal strain curve measured after several load–unload cycles is illustrated in Fig. 4(a). Points A–F in Fig. 4(a) correspond to the same points in Fig. 3. At point A the electric field is zero and the sample has a remanent longitudinal strain of 0.0027. As the positive electric field (opposite to the direction of polarization) is applied, the domains in the sample are constricted by the dielectric effect and the longitudinal strain is reduced. At point B, the electric field reaches the coercive field and the polarization switches to the direction of the electric field. The longitudinal strain increases suddenly. At point C the polarization has switched completely and the strain varies approximately linearly with the electric field. As the electric field decreases to zero at point D, the strain returns to that of point A. When a negative electric field (opposite to the current direction of the polarization) is applied to the sample, due to the dielectric effect, the sample is constricted along the direction of the electric field. The longitudinal strain is reduced. At point E the electric field reaches the coercive field and the strain increases quickly for the polarization switching. The switch is completed at point F. As the electric field decreases to zero, the sample returns to the state of

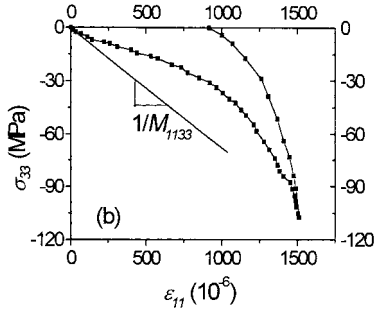

Fig. 5. Uniaxial compressive stress vs transverse strain curve.

point A and the sequent cycles are followed in the same way. When the electric field is zero (such as at points A and D), the small change of the longitudinal strain is linearly proportional to the small change of the electric field. This phenomenon can be described by $\Delta\varepsilon_{33} = d_{333}\Delta E_3$. The stable butterfly shaped transverse strain vs electric field hysteresis loop measured after several load–unload cycles, as demonstrated in Fig. 4(b), indicates that the transverse strain, ε_{11}, varies nonlinearly with the electric field, E_3, as well and the amplitude is about minus one half of that of the longitudinal strain. The linear piezoelectric coefficient, d_{311}, can be obtained from the slope at the point of zero electric field.

A compressive stress, σ_{33}, is applied to the sample in the polarization direction parallel to the x_3-axis. Figure 5 shows the transverse strain, ε_{11}, vs stress, σ_{33}, curve (the longitudinal strain, ε_{33}, vs stress, σ_{33}, curve is presented in Section 5 for comparison with the theoretical calculation), illustrating that the soft PZT-51 ceramic exhibits linear compressive strain when the uniaxial stress is under 10 MPa. As the stress exceeds 10 MPa, the polarization begins to switch and the sample shows nonlinear deformation. This is in full agreement with the results given by Cao and Evans [9]. After unloading from 110 MPa, the domains partially switch back to their original poling direction and there is a large rema-

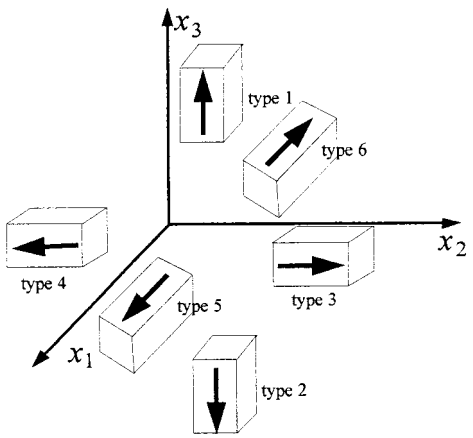

Fig. 6. Six domain types.

nent longitudinal strain, $\bar{\varepsilon}^{\mathrm{r}}_{33}$, and a remanent transverse strain, $\bar{\varepsilon}^{\mathrm{r}}_{11}$. The initial slope relating the uniaxial stress to the transverse strain is the inverse of the compliance M_{1133} as shown in Fig. 5. Similarly, the compliance M_{3333} can be obtained from the reverse of the initial slope of the longitudinal strain vs stress curve.

4. A DOMAIN SWITCHING MODEL

4.1. Description of domains and their orientations

As shown in Fig. 1, a unit cell of $BaTiO_3$, PZT and PLZT, etc. is cubic with edge length a_0 in the paraelectric phase. When phase transition occurs and the ceramic changes to the ferroelectric phase, the edges of the unit cell contract in two directions with their lengths changing from a_0 to a and elongate in one direction with its length changing from a_0 to c. If we choose the prototype phase as a reference state, this shape change causes a spontaneous strain. The relative displacements of ions in a unit cell lead to a spontaneous polarization as well. A ferroelectric domain in ferroelectric ceramics is composed of unit cells with the same spontaneous polarization. A unit cell may be seen as a representation of the domain that it belongs to.

Two coordinate systems, i.e. fixed local coordinates and fixed global coordinates, are used in this paper. All the physical quantities should be transformed into global coordinates before operation. We introduce the local coordinates because a domain switching has a relatively simple expression in its local coordinates. A set of fixed local coordinates, x_i, with the unit base vectors, $\mathbf{e}_i$, is associated with each domain in accordance with its spontaneous polarization. The three local coordinate axes are along the edges of the unit cell, and $\mathbf{e}_3$ is chosen along the direction of the spontaneous polarization. We call it a fixed local coordinate because once it is set, it does not change with domain switching. We will later refer to it as the "local coordinate" and do not specify the word "fixed". We designate the domain distribution in a ceramic at the beginning of the calculation as the initial domain distribution and the state of the domain as the initial state. The local coordinates are chosen at this moment and then fixed. Domain switching does not change the directions of the (fixed) local coordinates.

A domain of $BaTiO_3$, PZT and PLZT, etc. perovskite type ceramics has six variants according to its direction of polarization and can change from one variant to another. According to the definition of the local coordinates, the spontaneous polarization of a domain in the initial state is along $\mathbf{e}_3$. We specify it as type 1 domain (see Fig. 6). It is easy to see that a ceramic is initially made up of type 1 domains. Other types of domains are defined relative to the local coordinate. The domain types are schematically shown in Fig. 6. A type 2 domain has its spontaneous polarization along the opposite direction of $\mathbf{e}_3$. A type 3 domain has its spontaneous polarization along the direction of $\mathbf{e}_2$ and a type 4 domain the opposite. A type 5 domain has its spontaneous polarization along the direction of $\mathbf{e}_1$ and a type 6 domain the opposite. Domain switching is expressed in its local coordinates by domain type changes and the type 1 domain is the start of the history of domain type evolution. The domain distributions in a ceramic can be depicted by the domain type at each set of local coordinates. It should be clearly noted that such a specification of domain types is only valid for ferroelectric ceramics with a tetragonal structure.

A set of fixed global Cartesian coordinates X_I with its base vectors $\bar{\mathbf{e}}_I$ is defined as a reference. The local Cartesian coordinates are related to the global coordinate through the following transformation:

$$x_i = R_{iJ} X_J \tag{1}$$

where $R_{iJ} = \mathbf{e}_i \cdot \bar{\mathbf{e}}_J$ are the direction cosines between the local and global coordinates. R_{iJ} can also be expressed by three Euler angles as follows:

$$[R_{iJ}] = \begin{bmatrix} \cos\theta\cos\varphi\cos\psi - \sin\varphi\sin\psi & \cos\theta\sin\varphi\cos\psi + \cos\varphi\sin\psi & -\sin\theta\cos\psi \\ -\cos\theta\cos\varphi\sin\psi - \sin\varphi\cos\psi & -\cos\theta\sin\varphi\sin\psi + \cos\varphi\cos\psi & \sin\theta\sin\psi \\ \sin\theta\cos\varphi & \sin\theta\sin\varphi & \cos\theta \end{bmatrix} \tag{2}$$

where θ, φ, ψ are three Euler angles, as shown in Fig. 7. $\mathbf{R} = R_{iJ}\bar{\mathbf{e}}_I\bar{\mathbf{e}}_J$ ($i = I$, $j = J$ sum for I, J) is called the domain orientation tensor, analogous to what is defined in martensitic transformation crystallography [33]. The tensor, $\mathbf{R}$, actually defines a rotation. It turns the global unit base vector $\bar{\mathbf{e}}_I$ to the corresponding local unit base vector $\mathbf{e}_i = \mathbf{R} \cdot \bar{\mathbf{e}}_I$ ($i = I$). So $\mathbf{e}_i$ is a function of $\mathbf{R}$ and can be written as $\mathbf{e}_i = \mathbf{e}_i(\mathbf{R})$. It can be seen from equation (2) that there are three independent parameters θ, φ, ψ in the expression of $\mathbf{R}$ and $\mathbf{R} = \mathbf{R}(\theta, \varphi, \psi)$.

The orientation distribution function (ODF) is introduced to depict the domain patterns in a ferroelectric ceramic. That is, we have $f = f(\mathbf{R})$ or $f = f(\theta, \varphi, \psi)$. Thus, $f(\theta, \varphi, \psi)\sin\theta\, \mathrm{d}\psi\, \mathrm{d}\varphi\, \mathrm{d}\theta$ is the

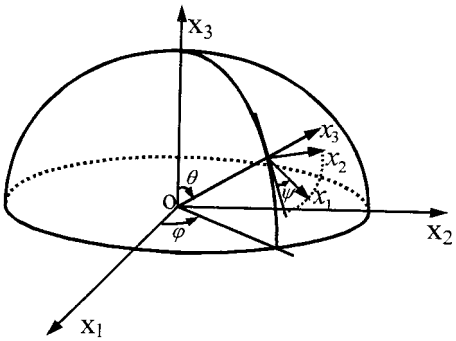

Fig. 7. Three Euler angles and the relation of coordinates.

volume fraction of domains whose orientation lies in the infinitesimal orientation element $\sin\theta\,\mathrm{d}\psi\,\mathrm{d}\varphi\,\mathrm{d}\theta$ centered at (θ, φ, ψ). Upon integrating over all orientations, f should satisfy the following normalization condition:

$$\int_0^{\pi}\int_0^{2\pi}\int_0^{2\pi} f(\theta, \varphi, \psi)\sin\theta\,\mathrm{d}\psi\,\mathrm{d}\varphi\,\mathrm{d}\theta = 1. \tag{3}$$

In the initial state the ceramic is unpoled, the domains are randomly distributed and the ceramic does not show any macroscopic polarization. In this case no orientation is more favorable than others and domains are evenly distributed in all orientations. So f is a constant over the three Euler angles θ, φ, ψ. From equation (3) we can obtain that $f = 1/8\pi^2$.

When there is no external stress and electric field, a ferroelectric domain still exhibits polarization and strain, which are called spontaneous polarization and spontaneous strain. As we have stated in Section 1, they come from phase transition. We will always use another term "spontaneous electric displacement" in this paper. It is defined as the electric displacement under null external electric field and stress. In physics the electric displacement is defined as $\mathbf{D} = \varepsilon_0\mathbf{E} + \mathbf{P}$, where ε_0 is the dielectric permittivity in vacuum, $\mathbf{D}$ the electric displacement, $\mathbf{E}$ the electric field and $\mathbf{P}$ the polarization. It is easy to see that the spontaneous electric displacement is equal to the spontaneous polarization. In order to distinguish the spontaneous quantities from other quantities, we use the superscript "*" to denote the spontaneous ones.

The spontaneous electric displacement and spontaneous strain of type 1 domain at orientation $\mathbf{R}$ can be expressed as follows (superscript 1 denoting the type $S = 1$):

$$\begin{aligned}\mathbf{D}^*(\mathbf{R};1) &= D_i^{*1}\mathbf{e}_i(\mathbf{R}) = P^0\mathbf{e}_3,\\ \boldsymbol{\varepsilon}^*(\mathbf{R};1) &= \varepsilon_{ij}^{*1}\mathbf{e}_i(\mathbf{R})\mathbf{e}_j(\mathbf{R})\\ &= (a-a_0)/a_0\mathbf{e}_1\mathbf{e}_1 + (a-a_0)/a_0\mathbf{e}_2\mathbf{e}_2\\ &\quad + (c-a_0)/a_0\mathbf{e}_3\mathbf{e}_3\end{aligned} \tag{4}$$

where $\mathbf{D}^*(\mathbf{R};1)$ and $\boldsymbol{\varepsilon}^*(\mathbf{R};1)$ are the spontaneous electric displacement and the spontaneous strain of the type 1 domain at orientation $\mathbf{R}$, respectively. P^0 is the magnitude of spontaneous polarization, a_0 the lattice constant of the cubic cell and a, c are the constants of the tetragonal cell. The elastic compliance, $\mathbf{M}(\mathbf{R};1)$, the piezoelectric compliance, $\mathbf{d}(\mathbf{R};1)$, and the dielectric permittivity, $\mathbf{k}(\mathbf{R};1)$, of type 1 domain at orientation $\mathbf{R}$ are expressed by

$$\begin{aligned}\mathbf{M}(\mathbf{R};1) &= M^{\,1}_{ijkl}\mathbf{e}_i(\mathbf{R})\mathbf{e}_j(\mathbf{R})\mathbf{e}_k(\mathbf{R})\mathbf{e}_l(\mathbf{R}),\\ \mathbf{d}(\mathbf{R};1) &= d^1_{ijk}\mathbf{e}_i(\mathbf{R})\mathbf{e}_j(\mathbf{R})\mathbf{e}_k(\mathbf{R}),\\ \mathbf{k}(\mathbf{R};1) &= k^1_{ij}\mathbf{e}_i(\mathbf{R})\mathbf{e}_j(\mathbf{R}).\end{aligned} \tag{5}$$

The parameters of all other types (types 2–5) of domains at orientation $\mathbf{R}$ can be obtained through coordinate transformation.

The relations between type 1 domain and other types of domains are illustrated in Fig. 8. A type 2 domain can be obtained by a 180° rotation of a type 1 domain around the x_1-axis of local coordinates. A type 3 domain can be obtained by a –90° rotation of a type 1 domain around the x_1-axis of

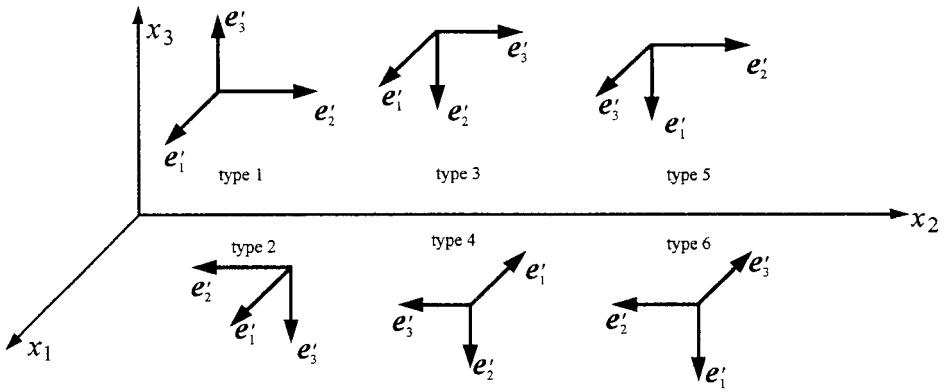

Fig. 8. The relation of the local coordinates and the co-switching coordinates.

the local coordinates. A type 4 domain can be obtained from a type 3 domain by a further 180° rotation around the x_3-axis of local coordinates. A type 5 domain can be obtained by a 90° rotation of a type 1 domain around the x_2-axis of local coordinates. A type 6 domain can be obtained from a type 5 domain by a further 180° rotation around the x_3-axis of local coordinates. It should be noted that such relations between a type 1 domain and other types of domains are restricted to ferroelectric materials exhibiting transformation from cubic to tetragonal only. In Fig. 8 we attach co-switching local Cartesian coordinates x_i' with the unit base vector $\mathbf{e}_i'(\mathbf{R})$ to each type of domain. $\mathbf{e}_3'(\mathbf{R})$ always points in the direction of polarization, and $\mathbf{e}_1'(\mathbf{R})$, $\mathbf{e}_2'(\mathbf{R})$ are arbitrarily chosen due to symmetry. For a type 1 domain, $\mathbf{e}_i'(1) = \mathbf{e}_i$. Evidently the material tensors [as in equation (5)] and spontaneous quantities (e.g. $\mathbf{D}^*$, $\boldsymbol{\varepsilon}^*$) for various types of domains have the same components in the co-switching coordinates.

Let S $(S = 1, 2, \ldots, 6)$ denote the type of domains. The components of tensors $\mathbf{D}^*(\mathbf{R}; S) = D_i^{*S}\mathbf{e}_i(\mathbf{R})$, $\boldsymbol{\varepsilon}^*(\mathbf{R}; S) = \varepsilon_{ij}^{*S}\mathbf{e}_i(\mathbf{R})\mathbf{e}_j(\mathbf{R})$, $\mathbf{M}(\mathbf{R}; S) = M^S_{ijkl}\mathbf{e}_i(\mathbf{R})\mathbf{e}_j(\mathbf{R})\mathbf{e}_k(\mathbf{R})\mathbf{e}_l(\mathbf{R})$, $\mathbf{d}(\mathbf{R}; S) = d^S_{ijk}\mathbf{e}_i(\mathbf{R})\mathbf{e}_j(\mathbf{R})\mathbf{e}_k(\mathbf{R})$, $\mathbf{k}(\mathbf{R}; S) = k^S_{ij}\mathbf{e}_i(\mathbf{R})\mathbf{e}_j(\mathbf{R})$ are related to those of type 1 domain through the following relations:

$$D^{*S}{}_i = T^S_{im} D^{*1}_m,\ \varepsilon^{*S}_{ij} = T^S_{im} T^S_{jn} \varepsilon^{*1}_{mn},$$

$$M^S_{ijkl} = T^S_{im} T^S_{jn} T^S_{ko} T^S_{lp} M^1_{mnop},$$

$$d^S_{ijk} = T^S_{im} T^S_{jn} T^S_{ko} d^1_{mno},\ k^S_{ij} = T^S_{im} T^S_{jn} k^1_{mn} \tag{6}$$

where

$$[T^1_{im}] = \begin{bmatrix} 1 & 0 & 0 \\ 0 & 1 & 0 \\ 0 & 0 & 1 \end{bmatrix},$$

$$[T^2_{im}] = \begin{bmatrix} 1 & 0 & 0 \\ 0 & -1 & 0 \\ 0 & 0 & -1 \end{bmatrix},$$

$$[T^3_{im}] = \begin{bmatrix} 1 & 0 & 0 \\ 0 & 0 & 1 \\ 0 & -1 & 0 \end{bmatrix},$$

$$[T^4_{im}] = \begin{bmatrix} -1 & 0 & 0 \\ 0 & 0 & -1 \\ 0 & -1 & 0 \end{bmatrix},$$

$$[T^5_{im}] = \begin{bmatrix} 0 & 0 & 1 \\ 0 & 1 & 0 \\ -1 & 0 & 0 \end{bmatrix},$$

$$[T^6_{im}] = \begin{bmatrix} 0 & 0 & -1 \\ 0 & -1 & 0 \\ -1 & 0 & 0 \end{bmatrix}. \tag{7}$$

The co-switching coordinates introduced here are only used to obtain the expressions of the components of $\mathbf{D}^*(\mathbf{R}; S)$, $\boldsymbol{\varepsilon}^*(\mathbf{R}; S)$, $\mathbf{M}(\mathbf{R}; S)$, $\mathbf{d}(\mathbf{R}; S)$, $\mathbf{k}(\mathbf{R}; S)$ in the local coordinates. To any $\mathbf{R}$ there corresponds a set of local coordinates. The S at this $\mathbf{R}$, which we denote by $S(\mathbf{R})$, determines the domain type. If the domain types at any $\mathbf{R}$, i.e. $S(\mathbf{R})$, are known, the whole domain patterns in the ceramic are clear. The domain type $S(\mathbf{R})$ changes during domain switching. To obtain the evolution of $S(\mathbf{R})$ is an important effort in this paper. All the quantities expressed in the local coordinates can be transformed into the global coordinate by the tensor transformation law. (See equations (1) and (2).)

4.2. Energy and switching criteria

The strain and the electric displacement in a domain come from two sources. One contribution is the spontaneous strain and electric displacement. The other contribution is strain and electric displacement induced by stress and electric field. So the piezoelectric equation in a domain can be written as

$$\boldsymbol{\varepsilon} = \boldsymbol{\varepsilon}^* + \mathbf{M}{:}\boldsymbol{\sigma} + \mathbf{E}\cdot\mathbf{d},\ \mathbf{D} = \mathbf{D}^* + \mathbf{d}{:}\boldsymbol{\sigma} + \mathbf{k}\cdot\mathbf{E}. \tag{8}$$

It should be emphasized that $\boldsymbol{\varepsilon}^*$, $\mathbf{D}^*$, $\mathbf{M}$, $\mathbf{d}$, $\mathbf{k}$ are related to $\mathbf{R}$ and S. It can be seen from equation (8) that there are two sources of the nonlinear behavior of a domain. One is the direct change of the spontaneous strain, $\boldsymbol{\varepsilon}^*$, and the electric displacement, $\mathbf{D}^*$, during domain switching. The other is the change of $\mathbf{M}$, $\mathbf{d}$, $\mathbf{k}$, as well as the additional change of strain and electric displacement through either a mechanical effect or electric effect, and/or the coupling of the two.

We suppose the temperature is constant during domain switching. At a certain temperature, the Gibbs free energy density, which is denoted by g, is a function of $\mathbf{R}$, $\boldsymbol{\sigma}$, $\mathbf{E}$, S, i.e. $g = g(\mathbf{R}; \boldsymbol{\sigma}, \mathbf{E}, S)$. According to the second law of thermodynamics, a state with a higher Gibbs energy tends to change to the state with a lower Gibbs free energy. The difference of the Gibbs energy of two states is the domain switching driving force. When the force exceeds certain thresholds, domain switching will occur. According to the thermodynamics law, when temperature is constant, the Gibbs free energy (per unit volume) in a domain can be expressed as

$$g = -\int_0^{\boldsymbol{\sigma}} \boldsymbol{\varepsilon}{:}\mathrm{d}\boldsymbol{\sigma} - \int_0^{\mathbf{E}} \mathbf{D}\cdot\mathrm{d}\mathbf{E}. \tag{9}$$

From equations (8) and (9), we have

$$g = -\left(\boldsymbol{\varepsilon}^*{:}\boldsymbol{\sigma} + \mathbf{D}^*\cdot\mathbf{E} + \frac{1}{2}\boldsymbol{\sigma}{:}\mathbf{M}{:}\boldsymbol{\sigma} + \frac{1}{2}\mathbf{E}\cdot\mathbf{k}\cdot\mathbf{E} + \mathbf{E}\cdot\mathbf{d}{:}\boldsymbol{\sigma}\right). \tag{10}$$

Equation (10) shows that the Gibbs free energy in a domain, g, is determined by external loads and parameters $\boldsymbol{\varepsilon}^*$, $\mathbf{D}^*$, $\mathbf{M}$, $\mathbf{k}$, $\mathbf{d}$. When the external loads, $\boldsymbol{\sigma}(t)$, $\mathbf{E}(t)$, are given, $\boldsymbol{\varepsilon}^*$, $\mathbf{D}^*$, $\mathbf{M}$, $\mathbf{k}$, $\mathbf{d}$, can be

obtained from equations (4)–(7). It should be noted that the domain type varies with time.

In the initial state (time $t = 0$, denoted by subscript "0"), according to the definition of the local coordinates, the domain type is 1 at any $\mathbf{R}$, i.e. $S_0(\mathbf{R}) = 1$. Equation (10) can finally give $g(\mathbf{R}; \boldsymbol{\sigma}_0, \mathbf{E}_0, S_0)$. Suppose at time t the Gibbs free energy is $g(\mathbf{R}; \boldsymbol{\sigma}_t, \mathbf{E}_t, S_t)$. At time $t + \mathrm{d}t$, if $S_{t+\mathrm{d}t}(\mathbf{R})$ is obtained, the Gibbs free energy $g(\mathbf{R}; \boldsymbol{\sigma}_{t+\mathrm{d}t}, \mathbf{E}_{t+\mathrm{d}t}, S_{t+\mathrm{d}t})$ can be calculated. $S_{t+\mathrm{d}t}(\mathbf{R})$ is obtained as follows.

At a certain $\mathbf{R}$, $S_{t+\mathrm{d}t}$ has six possible values, from 1 to 6. If $S_{t+\mathrm{d}t}$ remains the same as S_t, no domain switching occurs. Otherwise, domain switching appears. There is energy dissipation associated with domain switching, so the domain switching driving force must be greater than the threshold corresponding to switching. The thresholds for 90° and 180° domain switching are different and are denoted as W^f_{90} and W^f_{180}, respectively. Generally speaking, W^f_{90} and W^f_{180} are related to materials and may also be influenced by external loading. Here we suppose they are material constants. Domain type S is an element of set $\{A\}$, where $\{A\} = \{1, 2, 3, 4, 5, 6\}$. Let A^t_{180} denote the domain type 180° switching relative to domain type S_t. A^t_{180} can be determined in the following way. If S_t is an odd number, $A^t_{180} = S_t + 1$. If S_t is an even number, $A^t_{180} = S_t - 1$. For example, if $S_t = 3$ then $A^t_{180} = 4$. If $S_t = 6$ then $A^t_{180} = 5$. Let A^t_{90} denote those domain types of the 90° switching relative to domain type S_t. It is easy to see that $\{A^t_{90}\} = \{A\} - A^t_{180} - S_t$. For example, if $S_t = 3$, we can obtain that $A^t_{180} = 4$, so $\{A^t_{90}\} = \{1, 2, 5, 6\}$.

The domain switching driving force of 90° switching F_{90}, is defined as

$$F_{90}(\mathbf{R}; \boldsymbol{\sigma}_{t+\mathrm{d}t}, \mathbf{E}_{t+\mathrm{d}t}) = \max\{g(\boldsymbol{R}; \boldsymbol{\sigma}_t, \mathbf{E}_t, S_t) - g(\mathbf{R}; \boldsymbol{\sigma}_{t+\mathrm{d}t}, \mathbf{E}_{t+\mathrm{d}t}, S)\}_{S\in\{A^t_{90}\}}. \quad (11)$$

We use S^p_{90} to denote the S that satisfies the above definition of F_{90}. The domain switching driving force of 180° switching F_{180}, is defined as

$$F_{180}(\mathbf{R}; \boldsymbol{\sigma}_{t+\mathrm{d}t}, \mathbf{E}_{t+\mathrm{d}t}) = \max\{g(\boldsymbol{R}; \boldsymbol{\sigma}_t, \mathbf{E}_t, S_t) - g(\mathbf{R}; \boldsymbol{\sigma}_{t+\mathrm{d}t}, \mathbf{E}_{t+\mathrm{d}t}, S)\}_{S=A^t_{180}}. \quad (12)$$

We use S^p_{180} to denote the A^t_{180}. The domain switching criterion can be stated as follows:

if $F_{90}(\mathbf{R}; \boldsymbol{\sigma}_{t+\mathrm{d}t}, \mathbf{E}_{t+\mathrm{d}t}) \geq W^f_{90}$ then 90° domain switching occurs at orientation $\mathbf{R}$ and $S_{t+\mathrm{d}t} = S^p_{90}$, otherwise no domain switching occurs at orientation $\mathbf{R}$ and $S_{t+\mathrm{d}t} = S_t$;

if $F_{180}(\mathbf{R}; \boldsymbol{\sigma}_{t+\mathrm{d}t}, \mathbf{E}_{t+\mathrm{d}t}) \geq W^f_{180}$ then 180° domain switching occurs at orientation $\mathbf{R}$ and $S_{t+\mathrm{d}t} = S^p_{180}$, otherwise no domain switching occurs at orientation $\mathbf{R}$ and $S_{t+\mathrm{d}t} = S_t$.

When the evolution of $S(\mathbf{R})$ is known, we can obtain the macroscopic strain and electric displacement of the ceramic by averaging over all the domains.

4.3. Macroscopic strain and electric displacement

We have assumed that the domains are independent of each other, and the stress and electric field of each domain is equal to the external stress and electric field. The strain and electric displacement of each domain can be obtained from equation (8). The macroscopic strain and the electric displacement of the ceramic are obtained by averaging over all the domains. The expressions are as follows:

$$\begin{aligned}\bar{\boldsymbol{\varepsilon}} &= \frac{1}{V}\int_V \boldsymbol{\sigma}\,\mathrm{d}V \\ &= \int_0^{\pi}\int_0^{2\pi}\int_0^{2\pi} \boldsymbol{\sigma}(\theta, \varphi, \psi) f(\theta, \varphi, \psi)\sin\theta\,\mathrm{d}\psi\,\mathrm{d}\varphi\,\mathrm{d}\theta, \\ \bar{\mathbf{D}} &= \frac{1}{V}\int_V \mathbf{D}\,\mathrm{d}V \\ &= \int_0^{\pi}\int_0^{2\pi}\int_0^{2\pi} \mathbf{D}(\theta, \varphi, \psi) f(\theta, \varphi, \psi)\sin\theta\,\mathrm{d}\psi\,\mathrm{d}\varphi\,\mathrm{d}\theta.\end{aligned} \quad (13)$$

In an unpoled initial state, the domains are randomly distributed and the ceramic does not show any macroscopic polarization. If our calculation starts from this unpoled state, according to equation (3), f has a simple form: $f = 1/8\pi^2$. Then the macroscopic constitutive relation can be written as

$$\bar{\boldsymbol{\varepsilon}} = \bar{\boldsymbol{\varepsilon}}^* + \bar{\mathbf{M}}{:}\boldsymbol{\sigma} + \mathbf{E}\cdot\bar{\mathbf{d}},\ \bar{\mathbf{D}} = \bar{\mathbf{D}}^* + \bar{\mathbf{d}}{:}\boldsymbol{\sigma} + \bar{\mathbf{k}}\cdot\mathbf{E} \quad (14)$$

where

$$\begin{aligned}\bar{\boldsymbol{\varepsilon}}^* &= \frac{1}{8\pi^2}\int_0^{\pi}\int_0^{2\pi}\int_0^{2\pi} \boldsymbol{\varepsilon}^*(\theta, \varphi, \psi)\sin\theta\,\mathrm{d}\psi\,\mathrm{d}\varphi\,\mathrm{d}\theta, \\ \bar{\mathbf{M}} &= \frac{1}{8\pi^2}\int_0^{\pi}\int_0^{2\pi}\int_0^{2\pi} \mathbf{M}(\theta, \varphi, \psi)\sin\theta\,\mathrm{d}\psi\,\mathrm{d}\varphi\,\mathrm{d}\theta, \\ \bar{\mathbf{d}} &= \frac{1}{8\pi^2}\int_0^{\pi}\int_0^{2\pi}\int_0^{2\pi} \mathbf{d}(\theta, \varphi, \psi)\sin\theta\,\mathrm{d}\psi\,\mathrm{d}\varphi\,\mathrm{d}\theta, \\ \bar{\mathbf{D}}^* &= \frac{1}{8\pi^2}\int_0^{\pi}\int_0^{2\pi}\int_0^{2\pi} \mathbf{D}^*(\theta, \varphi, \psi)\sin\theta\,\mathrm{d}\psi\,\mathrm{d}\varphi\,\mathrm{d}\theta, \\ \bar{\mathbf{k}} &= \frac{1}{8\pi^2}\int_0^{\pi}\int_0^{2\pi}\int_0^{2\pi} \mathbf{k}(\theta, \varphi, \psi)\sin\theta\,\mathrm{d}\psi\,\mathrm{d}\varphi\,\mathrm{d}\theta.\end{aligned} \quad (15)$$

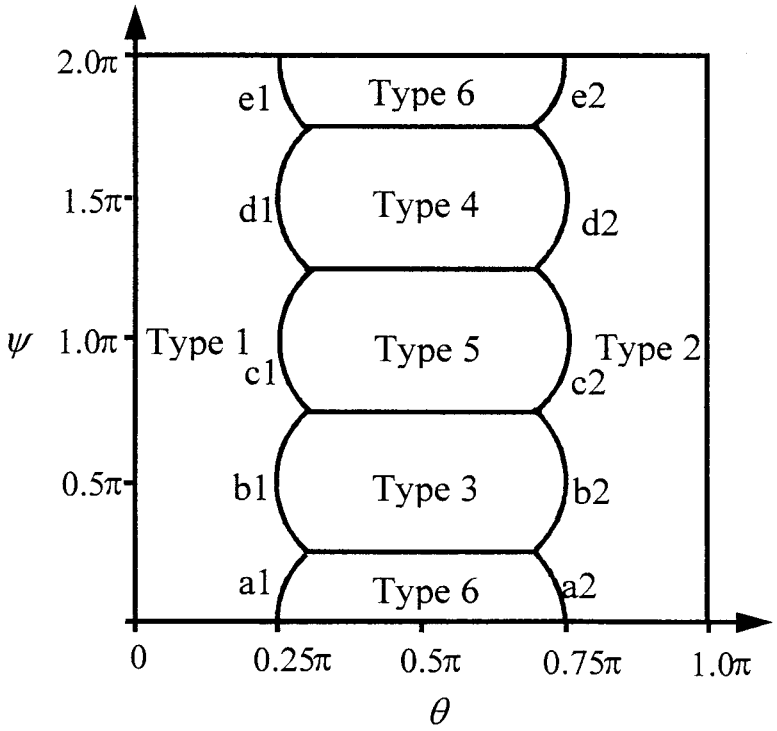

Fig. 9. Domain type distributions of a fully poled ceramic.

4.4. Relation between macroscopic and microscopic quantities

Based on the above theory, we can draw some useful conclusions. These conclusions can help us understand some general relations between the macroscopic and the microscopic quantities. Some microscopic quantities difficult to measure directly can be obtained through the relatively easy measurement of macroscopic quantities. In this section, we will discuss the relation of the magnitude of the spontaneous polarization to the remanent polarization of the ceramic, the relation of the components of the spontaneous strain to the remanent strain induced by the poling electric field, and the piezoelectric compliance of a domain to the macroscopic piezoelectric compliance. We will also determine the 90° and 180° domain switching thresholds W^f_{90} and W^f_{180}.

When a ceramic is fully poled, all the domains turn to the most favorable direction which is closest to the external electric field. This condition can determine the domain type S at any orientation θ, φ, ψ. Suppose the electric field is along $\bar{\mathbf{e}}_3$, the domain type $S(\theta, \varphi, \psi)$ at θ, φ, ψ maximizes the expression $\mathbf{D}^*(\theta, \varphi, \psi; S) \cdot \bar{\mathbf{e}}_3$. In other words, at any θ, φ, ψ we have

$$\mathbf{D}^*(\theta, \varphi, \psi; S(\theta, \varphi, \psi)) \cdot \bar{\mathbf{e}}_3 \geq \mathbf{D}^*(\theta, \varphi, \psi; S^i) \cdot \bar{\mathbf{e}}_3 \quad \forall S^i \in \{A\}. \tag{16}$$

Let us see the domain type distribution vs θ, φ, ψ. The values of $\mathbf{D}^*(\theta, \varphi, \psi; S^i) \cdot \bar{\mathbf{e}}_3$ ($S^i \in \{A\}$) can be obtained in terms of equations (1), (2), (6) and (7):

$$\begin{aligned}
&\mathbf{D}^*(\theta, \varphi, \psi; 1) \cdot \bar{\mathbf{e}}_3 = P^0 \cos\theta,\\
&\mathbf{D}^*(\theta, \varphi, \psi; 2) \cdot \bar{\mathbf{e}}_3 = -P^0 \cos\theta,\\
&\mathbf{D}^*(\theta, \varphi, \psi; 3) \cdot \bar{\mathbf{e}}_3 = P^0 \sin\theta \sin\psi,\\
&\mathbf{D}^*(\theta, \varphi, \psi; 4) \cdot \bar{\mathbf{e}}_3 = -P^0 \sin\theta \sin\psi,\\
&\mathbf{D}^*(\theta, \varphi, \psi; 5) \cdot \bar{\mathbf{e}}_3 = -P^0 \sin\theta \cos\psi,\\
&\mathbf{D}^*(\theta, \varphi, \psi; 6) \cdot \bar{\mathbf{e}}_3 = P^0 \sin\theta \cos\psi.
\end{aligned} \tag{17}$$

From equations (16) and (17) we can get the domain type distribution vs θ, φ, ψ as shown in Fig. 9. The equations of bordering curves in Fig. 9 are expressed as follows [28]:

a1: $\cos\theta = \sin\theta\cos\psi \ \ (0 \le \psi \le 1/4\pi)$,

a2: $-\cos\theta = \sin\theta\cos\psi \ \ (0 \le \psi \le 1/4\pi)$,

b1: $\cos\theta = \sin\theta\sin\psi \ \ (1/4\pi \le \psi \le 3/4\pi)$,

b2: $-\cos\theta = \sin\theta\sin\psi \ \ (1/4\pi \le \psi \le 3/4\pi)$,

c1: $\cos\theta = -\sin s\cos\psi \ \ (3/4\pi \le \psi \le 5/4\pi)$,

c2: $\cos\theta = \sin s\cos\psi \ \ (3/4\pi \le \psi \le 5/4\pi)$,

d1: $\cos\theta = -\sin\theta\sin\psi \ \ (5/4\pi \le \psi \le 7/4\pi)$,

d2: $\cos\theta = \sin\theta\sin\psi \ \ (5/4\pi \le \psi \le 7/4\pi)$,

e1: $\cos\theta = \sin\theta\cos\psi \ \ (7/4\pi \le \psi \le 2\pi)$,

e2: $-\cos\theta = \sin\theta\cos\psi \ \ (7/4\pi \le \psi \le 2\pi)$. (18)

Note that in terms of equations (16) and (17) equation (18) can be obtained by letting each subequation in equation (17) be equal to other subequations of equation (17). Since $S(\theta, \varphi, \psi)$ is known, the macroscopic quantities can be obtained through averaging. When the ceramic is fully poled by an electric field and then the electric field decreases to zero, a remanent polarization and strain are induced. In terms of equation (15), the magnitude of the remanent polarization, P^{R}, could be obtained as [28]

$$P^{\mathrm{R}} = \frac{1}{8\pi^2}\int_0^{\pi}\int_0^{2\pi}\int_0^{2\pi} \mathbf{D}^{*}(\theta, \varphi, \psi; S^{\mathrm{R}}) \cdot \bar{\mathbf{e}}_3 \sin\theta \, \mathrm{d}\psi \, \mathrm{d}\varphi \, \mathrm{d}\theta = 0.831P^0 \tag{19}$$

where $S^{\mathrm{R}}(\theta, \varphi, \psi)$ is the domain type distribution shown in Fig. 9. Similarly, the remanent strain can be obtained as

Applying equations (12) and (10) to the 180° switching induced by electric field, the maximum driving force for 180° switching is $2P^0E$. Let E_{c} be the coercive electric field. From the domain switching criterion [see equation (12)] in Section 4.2, we can obtain the 180° domain switching friction as [28]

$$W^{f}_{180} = 2P^0E_{\mathrm{c}}. \tag{21}$$

Similarly, applying equations (11) and (10) to the 90° switching induced by compressive stress and letting the applied stress σ be equal to the coercive stress, σ_{c}, we can obtain the 90° domain switching friction expressed by

$$W^{f}_{90} = \left(\frac{c-a}{a_0}\right)\sigma_{\mathrm{c}} + \frac{1}{2}(M_{1111} - M_{3333})\sigma_{\mathrm{c}}^2 \tag{22}$$

where M_{1111} and M_{3333} are components of the elastic compliance in the x_1- and x_3-directions, respectively.

5. COMPARISON OF THEORY AND EXPERIMENT

In this section, we present our numerical calculation results and then compare them both with experimental results on ceramic lead lanthanum zirconate titanate (PLZT) obtained by Hwang *et al.* [20] and with our experimental data on the soft PZT-51 ceramic subjected to the combined electric–mechanical loading [32]. The material properties of the PZT ceramic are listed in Tables 1 and 2 [32] and the material properties of the PLZT ceramic can be found in Ref. [20].

First we compare the theoretical calculation with the experiments done by Hwang *et al.* [20]. The ceramic is initially unpoled, then an electric field $\mathbf{E} = A\sin((k/N_E)\pi)\bar{\mathbf{e}}_3$ is applied, where $A = 1.0$ MV/m, $N_E = 200$, $k = 0, 1, 2, \ldots, 4000$. Hwang *et al.* [20] proposed such a domain switching criterion as

$$E_i\Delta P_i + \sigma_{jk}\Delta\varepsilon_{jk} \ge 2P^0E_{\mathrm{c}} \tag{23}$$

where ΔP_i is the change in the spontaneous polarization, $\Delta\varepsilon_{jk}$ the change in the spontaneous strain, and P^0 the magnitude of the spontaneous polarization. Based on this criterion, Hwang *et al.* [20]

$$[\bar{\varepsilon}^{\mathrm{R}}_{IJ}] = \frac{1}{8\pi^2}\int_0^{\pi}\int_0^{2\pi}\int_0^{2\pi} \bar{\mathbf{e}}_I \cdot \bar{\boldsymbol{\varepsilon}}^{*}(\theta, \varphi, \psi; S^{\mathrm{R}}) \cdot \bar{\mathbf{e}}_J \sin\theta \, \mathrm{d}\psi \, \mathrm{d}\varphi \, \mathrm{d}\theta$$

$$= \begin{bmatrix} 0.85048\left(\dfrac{a-a_0}{a_0}\right) + 0.14952\left(\dfrac{c-a_0}{a_0}\right) & 0 & 0 \\ 0 & 0.85048\left(\dfrac{a-a_0}{a_0}\right) + 0.14952\left(\dfrac{c-a_0}{a_0}\right) & 0 \\ 0 & 0 & 0.29905\left(\dfrac{a-a_0}{a_0}\right) + 0.70095\left(\dfrac{c-a_0}{a_0}\right) \end{bmatrix}. \tag{20}$$

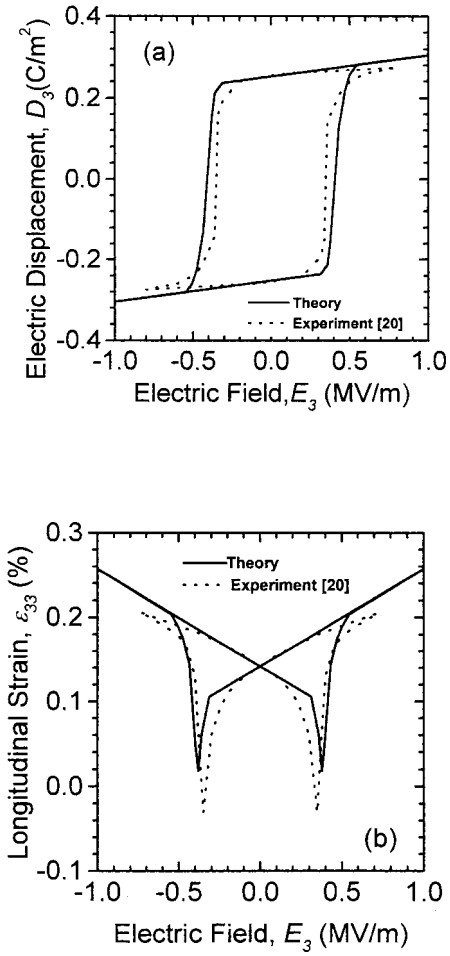

Fig. 10. Comparison of theory and experiment [20] based on the separate 180° and 90° domain switching criteria: (a) electric displacement vs electric field curves for PLZT; (b) longitudinal strain vs electric field curves for PLZT. Experimental data are obtained from Ref. [20].

compared their calculations with the experimental results. It was found that their model cannot describe the relation between longitudinal strain and electric field (see Fig. 10 of Ref. [20]). The predictd value of the strain at the moment of the domain switching is much less than that of the measured strain. In order to examine the effect of the domain switching criterion on the macroscopic behavior, we use different domain switching criteria in the calculation. When the 90° domain switching friction and 180° domain switching friction are taken the same as in equation (21), we find that the model cannot describe the relation between longitudinal strain and electric field as well. The prediction is exactly the same as that in Ref. [20]. It is interesting to find that the term on the right-hand side of equation (23) is the same as that on the right-hand side of equation (21). When only an electric field is applied, the second term on the left-hand side of equation (23) vanishes. Thus, from equations (12), (21) and (23), we could find that the 180° domain switching criterion is identical to the criterion of Hwang *et al.* [20]. Now we distinguish 90° and 180° domain switching frictions as presented in equations (21) and (22), and an obvious improvement in comparison of theoretical results and experiment is found as illustrated in Figs 10(a) and (b). It can be found that Fig. 10 shows much better agreement than that calculated by use of the 180° domain switching energy barrier, especially in the longitudinal strain vs electric field curves. The minimal value of the longitudinal strain in Fig. 10(b) is closer to the experimental result, while the longitudinal strain calculated by use of the 180° domain switching energy barrier gives a much higher minimal longitudinal strain. Many researchers [5–8] have found that domain wall movements can lead to the 90° or the 180° domain switching and their mechanisms are different. The above results agree with the observation of those researchers [5–8]. The differences in switching criteria for the electric field driven switching and stress driven switching suggest that there might be a different energy barrier for the 90° and the 180° switches, which may be explained by domain wall dynamics. The experimental results may further be understood by the proposed domain switching criteria. Switching is the source of the classic butterfly shaped strain vs electric field curve and the corresponding electric displacement vs electric field curve. It is also the source of the nonlinear stress–strain curve.

In the following, we shall compare numerical calculations with results of experiments on the soft PZT-51 ceramic, which were conducted in our Failure Mechanics Laboratory [32]. The material properties are listed in Table 1. The electric displacement vs electric field curves and longitudinal strain vs electric field curves under various compressive stresses are demonstrated in Figs 11(a)–(h), respectively. The solid lines represent theoretical results and the marked lines represent experimental results. Figure 11 shows that the model can characterize the electric–mechanical response and the effect on depolarization due to the compressive stress under the combined electric–mechanical loading.

In the case that the specimen is subjected to the combined electric–mechanical loads, a constant compressive stress is imposed in the polarization direction parallel to the x_3-axis while the electric field is cyclically applied. Figures 11(a), (c), (e) and (g) illustrate that D_3 vs E_3 hysteresis loops are developed at different constant compressive stress, indicating that there is a significant effect of the uniaxial compressive stress on the hysteresis behavior. The resulting hysteresis loops show a steady decrease in both the remanent polarization and the saturation polarization as the compressive stress is changed from 0 to −80 MPa. The slope of the loops at zero electrical field, which can be regarded as the permittivity, decreases when the magnitude of com-

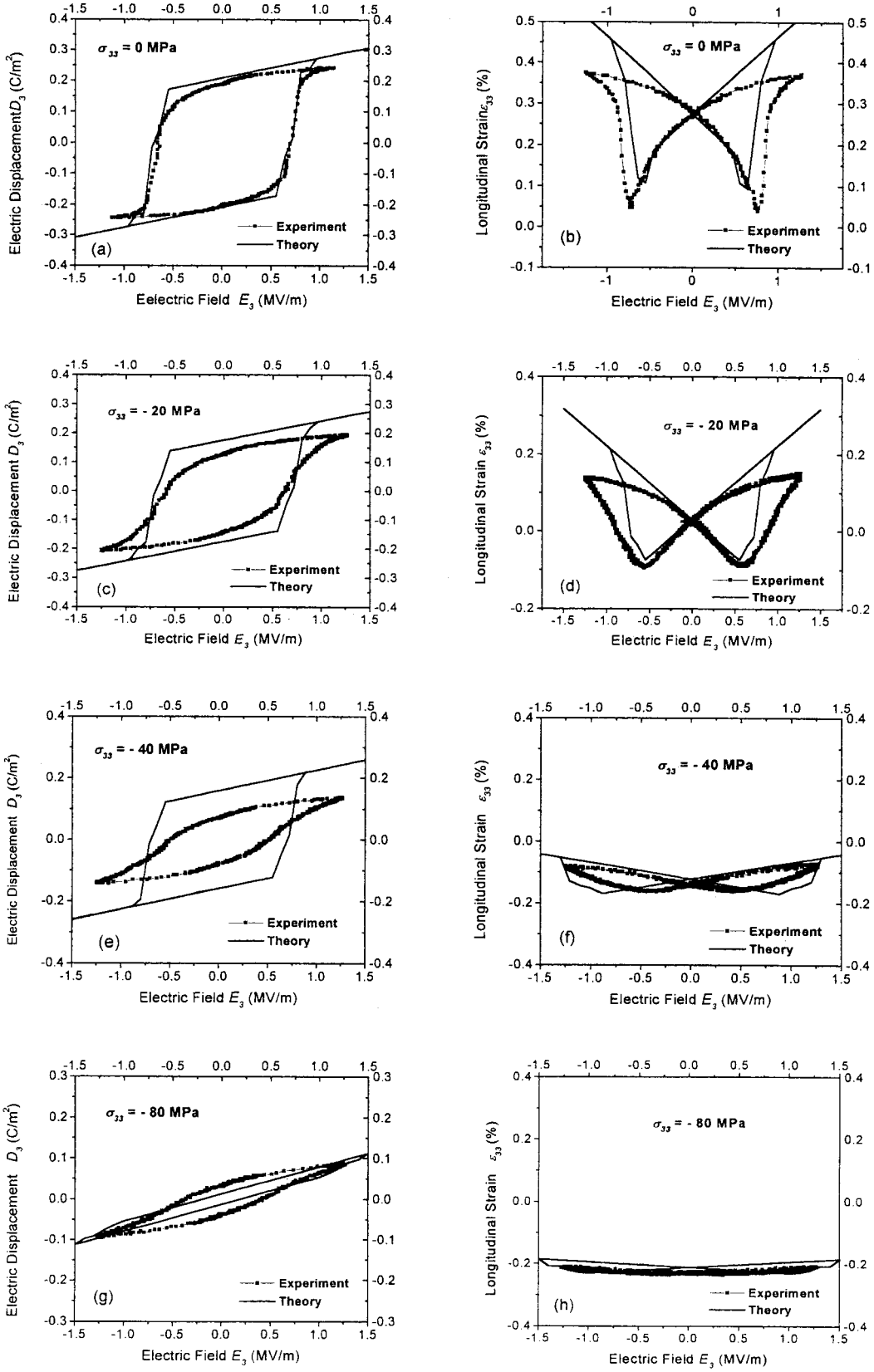

Fig. 11. Comparison of theory and experiment [32] for the case of the combined electric–mechanical loading: the axial compressive stress equals (a) and (b) 0 MPa; (c) and (d) −20 MPa; (e) and (f) −40 MPa; (g) and (h) −80 MPa, respectively.

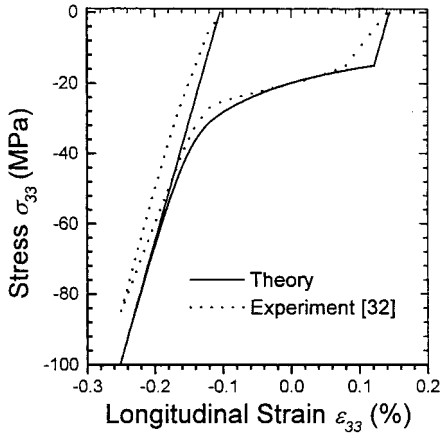

Fig. 12. Comparison of theory and experiment [32] based on the separate 180° and 90° domain switching criteria: applied compressive stress vs longitudinal strain curve.

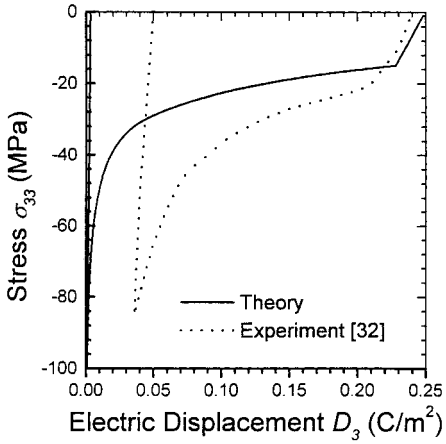

Fig. 13. Comparison of theory and experiment [32] based on the separate 180° and 90° domain switching criteria: applied compressive stress vs electric displacement curve.

pressive stress increases. The coercive field almost linearly decreases as the uniaxial compressive stress increases. This is the so-called depolarization phenomenon [9, 10], that is, when the magnitude of compressive stress increases, the remanent polarization decreases and the area encircled by the hysteresis decreases with the increase of compressive stress as well.

Similarly, the butterfly shaped longitudinal strain vs electric field curves are influenced by the external stress in such a way that they become flatter when the compresive stress increases. The longitudinal strain gradually becomes negative with reference to the unpolarized state when the compressive stress becomes larger. The range of the strain variation becomes smaller and smaller as the magnitude of compressive stress increases. And the range turns out to be almost zero when the stress goes over -80 MPa which is nearly the coercive stress field. This means that the domain switching becomes more difficult under a larger magnitude of compressive stress. The slope of the hoops at zero electrical field is not the piezoelectric coefficient but can be considered as the depolarization coefficient under different compressive stress levels. The slope is a function of the stress. The compressive stress acting in conjunction with the electric field induces 90° tetragonal switching. The ceramic remains in this 90° switched state until the electric field is sufficiently high to overcome the applied stress and switch the ceramic back to the polarized state. At a stress level of -80 MPa, the electric field is not able to totally overcome the applied stress and there is very little strain. There is still, however, a noticeable component of polarization switching though it is very small.

Finally, we shall make a comparison of stress vs strain. After the sample is poled, a compressive stress, $\sigma = B(k\pi/N_\sigma)\bar{\mathbf{e}}_3\bar{\mathbf{e}}_3$, is applied in the x_3-direction, where $B = 100$ MPa, $N_\sigma = 100$, $k = 1, 2, \ldots, 99, 100, 99, \ldots, 2, 1$. Figure 12 illustrates the comparison of applied compressive stress vs longitudinal strain curves of theory and experiment [32] based on the separate 180° and 90° domain switching criteria. Figure 13 demonstrates the comparison of applied compressive stress vs electric displacement curves of theory and experiment [32] based on the separate 180° and 90° domain switching criteria. The results in these two figures make it clear that the model could not describe the behavior of the stress vs electric displacement well though there does exist an agreement of theoretical and experimental stress vs strain curves.

6. CONCLUSIONS

External loads, such as electric field and stress, can cause domain switching. Domain switching always results in the nonlinear ferroelectricity and ferroelasticity of ferroelectric ceramics. A domain has different Gibbs energy at different orientation states and the energy difference forms the domain switching driving force. As long as the orientation of each domain is defined by its local coordinates relative to a set of fixed global coordinates, ODF can be simply employed to describe the domain pattern. The domain pattern and its evolution can be determined by the competition of the domain switching driving force and the dissipation during domain switching. The 90° and 180° domain switchings play different roles in ferroelectricity and ferroelasticity and have different switching dissipations associated with them. A criterion considering the difference of 90° and 180° switchings has been established by the thermodynamic approach. The results show that a better agreement of the calculations and experiments is achieved when the thresholds for 90° or 180° domain switchings are distinguished. The difference in switching criteria for the electric field driven switching and stress driven switching suggests that there might be different

energy barriers for the 90° switching and the 180° switching, which may be explained by domain wall dynamics. The experimental results may further be understood by the proposed domain switching criteria. Switching is the source of the classic butterfly shaped strain vs electric field curve and the corresponding electric displacement vs electric field curve. It is also the source of the nonlinear stress–strain curve. Both the theoretical prediction and the experimental measurement show that under the combined electric–mechanical loading, a compressive stress can reduce the polarization, leading to significant depolarization. That is, the electric–mechanical coupled behavior of the ferroelectric ceramic demonstrates that both the coercive field and the saturated field decrease as the compressive stress field increases. Furthermore, a sufficiently large compressive stress can even completely sweep off the butterfly shaped strain vs electric field hysteresis loop. Comparison of theoretical results and experimental results indicates that the proposed constitutive model can predict the main features of nonlinearity under combined loadings of electric field and stress. However, since the micromechanical model proposed in this paper is restricted to ferroelectric materials exhibiting transformation from cubic to tetragonal only, under the same principle of guidance, work still needs to be carried out to develop constitutive theories for other kinds of ferroelectric materials.

Acknowledgements—Support from the National Science Foundation of China under grants #19891180 and the State Education Commission of China is acknowledged. Japan Society for the Promotion of Science (JSPS ID No. S-97341) and T. Inoue are acknowledged for support to K.C.H.

REFERENCES

1. Lines, M. E. and Glass, A. M., *Principles and Applications of Ferroelectrics and Related Materials*. Oxford University Press, Oxford, 1977.
2. Haertling, G. H., *Ferroelectrics*, 1987, **22**, 75.
3. Araujo, C. A., McMillan, L. D., Melnick, B. M., Cauchiaro, J. D. and Scott, J. F., *Ferroelectrics*, 1990, **104**, 241.
4. Bondurant, D., *Ferroelectrics*, 1990, **112**, 273.
5. Fesenko, E. G., Semenchev, A. F. and Gavrilyatchenko, V. G., *Ferroelectrics*, 1976, **13**, 471.
6. Fesenko, E. G., Martynenko, M. A., Gavrilyatchenko, V. G. and Semenchev, A. F., *Ferroelectrics*, 1974, **7**, 309.
7. Stadler, H. L., *J. appl. Phys*., 1958, **29**, 1485.
8. Miller, R. C., *Phys. Rev*., 1958, **111**, 736.
9. Cao, H. and Evans, A., *J. Am. Ceram. Soc*., 1993, **76**, 890.
10. Lynch, C. S., *Acta metall. mater*., 1996, **44**, 4137.
11. Gao, H. J., Zhang, T. Y. and Tong, P., *J. Mech. Phys. Solids*, 1997, **45**, 491.
12. McMeeking, R. M., *J. appl. Math. Phys*., 1989, **40**, 615.
13. Sosa, H., *Int. J. Solids Struct*., 1989, **28**, 491.
14. Pak, Y. E., *J. appl. Mech*., 1990, **57**, 647.
15. Suo, Z., Kuo, C. M., Barnet, D. M. and Willis, J. R., *J. Mech. Phys. Solids*, 1992, **40**, 739.
16. Park, S. B. and Sun, C. T., *J. Am. Ceram. Soc*., 1995, **78**, 1475.
17. Zhu, T. and Yang, W., *Acta mater*., 1997, **45**, 4695.
18. Suo, Z., Smart Struct. and Mater., ASME Aerospace Division, AD 24, 1991.
19. Yang, W. and Suo, Z., *J. Mech. Phys. Solids*, 1994, **42**, 649.
20. Hwang, S. C., Lynch, C. S. and McMeeking, R. M., *Acta metall. mater*., 1995, **43**, 2073.
21. Lynch, C. S. and McMeeking, R. M., *Ferroelectrics*, 1994, **160**, 177.
22. Huo, Y. Z. and Jiang, Q., *SPIE*, 1996, **2715**, 448.
23. Loge, R. E. and Suo, Z., *Acta mater*., 1996, **44**, 3429.
24. Chen, X., Fang, D. N. and Hwang, K. C., *Smart Mater. Struct*., 1997, **6**, 145.
25. Chen, X., Fang, D. N. and Hwang, K. C., *Acta mater*., 1997, **45**, 3181.
26. Lu, W., Fang, D. N. and Hwang, K. C., *Key Engng Mater*., 1997, **145**, 983.
27. Lu, W., Fang, D. N. and Hwang, K. C., *Commun. Nonlinear Sci. Numer. Simul*., 1997, **2**, 30.
28. Lu, W., Macroscopic and microscopic constitutive studies on ferroelectric materials and shape memory alloys. Doctoral dissertation, Tsinghua University, Beijing, 1998.
29. Michelitsch, T. and Kreher, W. S., *Acta mater*., 1998, **46**, 5085.
30. Hao, T. H., Gong, X. and Suo, Z., *J. Mech. Phys. Solids*, 1996, **44**, 23.
31. Hill, R., *J. Mech. Phys. Solids*, 1963, **11**, 357.
32. Li, C. Q., Experimental study on the constitutive relations and electric-induced fatigue of ferroelectric materials. Master's thesis, Tsinghua University, Beijing, 1998.
33. Patoor, E., Eberhardt, A. and Berveiller, M., *Acta metall*., 1987, **35**, 2779.